NanoWorld Journal

https://doi.org/10.17756/nwj.2024-s1-034

Research Article

Open Access

Synthesis, Properties, and Applications of Perovskite Phase $BaZrO_3$ for Solar Cell Applications

Ekta Tamrakar[1*], R.N. Patel[2], Arun Kumar[1], Raunak Kumar Tamrakar[3] and Kanchan Upadhyay[3]

[1]*Department of Electronics and Telecommunication Engineering, Chhattisgarh Swami Vivekanand Technical University, Bhilai, Chhattisgarh, India*

[2]*Department of Electrical Engineering, National Institute of Technology, Raipur, Chhattisgarh, India*

[3]*Department of Applied Physics, Bhilai Institute of Technology (Seth Balkrishan Memorial), Durg, Chhattisgarh, India*

[*]Correspondence to:
Ekta Tamrakar
Department of Electronics and Telecommunication Engineering,
Chhattisgarh Swami Vivekanand Technical University,
Bhilai, Chhattisgarh, India.
E-mail: ektatamrakar@gmail.com

Received: January 03, 2024
Accepted: March 13, 2024
Published: March 18, 2024

Citation: Tamrakar E, Patel RN, Kumar A, Tamrakar RK, Upadhyay K. 2024. Synthesis, Properties, and Applications of Perovskite Phase $BaZrO_3$ for Solar Cell Applications. *NanoWorld J* 10(S1): S194-S198.

Published by United Scientific Group

Abstract

Barium zirconate ($BaZrO_3$) is a class of perovskite material. Due to their cheap cost, excellent performance, and solution processability, organic/inorganic perovskites are promising materials for next-generation photovoltaics. Perovskites are used in tandem solar cells, building-integrated photovoltaics, space applications, energy storage systems, and photovoltaic-driven catalysis due to their unique properties and rapid advances in solar cell performance. This review highlights photovoltaic-integrated technology advances. Discussed are current and future issues and possible next-generation applications in various sectors. The solution combustion approach has been used to create a gadolinium activated $BaZrO_3$ phosphor. The X-ray diffraction (XRD) techniques pattern of prepared phosphor powder exhibits a pure cubic crystal structure. The surface structure phosphor is examined using scanning electron microscopy (SEM) and powder. The main band in the excitation spectra has a maximum at 254 nm. The emission spectrum shows a well-defined ultraviolet B (UVB) emission band with a maximum at 318 nm, which corresponds to the 6P7/2/8S7/2 transition, upon stimulation at 254 nm. Due to the emitted UVB emission prepared phosphor can be used as a potential candidate for the photodynamic therapy application.

Keywords

$BaZrO_3$:Eu^{3+}, Phosphor, Excitation spectrum, Emission spectrum, Rare earths

Introduction

Photoluminescence spectroscopy is a common semiconductor and perovskite solar cell characterization method. It may reveal recombination. kinetics, processes, and free charge carrier electrochemical potential in single semiconductor layers, layer stacks with transport layers, and entire solar cells. Photoluminescence evaluation and interpretation require proper excitation conditions, calibration, and approximations to the complex theory of radiative, non-radiative, interface, charge transfer, and photon recycling. This article describes photoluminescence analysis in $BaZrO_3$ perovskite compositions and the factors to consider.

Pure $BaZrO_3$ is a material that is well-known in the refractory industry. It is characterized by a high melting point, great mechanical capabilities, excellent chemical stability, and structural compatibility with a wide variety of elements [1-4]. In addition to this, its perovskite structure is as perfect as it can be. By doping B-site cations with aliovalent ions, however, materials based on $BaZrO_3$ can also demonstrate impressive protonic conduction at moderate temperatures (over 500 °C). Because of this, these components are fantastic options for electrochemical devices such as solid electrolytes to produce hydrogen, hydrogen and gas sensors, steam electrolyzers, and fuel cells.

Because of high melting point of 2920, $BaZrO_3$ is widely thought of as a potential refractory material [5, 6]. Despite claims of minimal corrosion, $BaZrO_3$ has recently attracted interest as a viable refractory material for melts of titanium nickel [7] and titanium aluminide [8]. In addition to extremely high temperatures, refractory materials commonly work in corrosive, erosive, and/or erosive conditions. High melting points, great processibilities, suitable particle sizes, and robust thermodynamic stability even at high temperatures are thus required of refractories. The performance of the refractory material is projected to degrade more at high temperatures the larger the fraction of unwanted secondary phases and, consequently, the wider the discrepancy between the desired and achieved phases. Thus, phase-pure material must be synthesized [9].

In numerous fuel cell studies, proton conductors have served as the electrolytes. For example, acceptor doped $BaZrO_3$ is reported to have greater chemical stability to carbon dioxide than barium cerate and to have a higher proton conductivity [10]. The proton conductor that has been found to have the highest measured conductivity is $BaZrO_3$ that has been doped with yttrium. Because of this, a great deal of research on PCFC that makes use of Y-doped $BaZrO_3$ has been published, particularly in the past few years [11]. Due to its better chemical stability, low thermal expansion coefficient, high bulk conductivity, and reduced activation energy, yttrium doped $BaZrO_3$ is viewed as a potential material option for PCFCs solution when compared to other proton conducting perovskites [12]. The provision of the appropriate substructure by optimizing ceramic manufacturing and avoiding any negative effects on the electrical characteristics is one of the most hopeful methods to improve the qualities of $BaZrO_3$. One of the most hopeful approaches to enhancing $BaZrO_3$ characteristics is this one. Several efforts have been made over the past few years to produce phase pure and modified $BaZrO_3$ using a broad range of production methods to create microcrystalline material.

$BaZrO_3$-based ceramics are suitable building blocks for a variety of microwave devices because of their low dielectric loss characteristics and consistent dielectric constant over a wide frequency range [12-17]. $BaZrO_3$ perovskite solids were typically made using the conventional ceramic method. The ceramic approach has several drawbacks, such as the requirement for comparatively high heat treatment (1200 - 1500 °C), uneven composition dispersion, and occasionally phase development that is undesirable [15].

It is currently possible to synthesize several perovskite nanomaterials with various characteristics utilizing a variety of biological, chemical, physical, and hybrid synthesis methods. However, the former is more costly, and the latter is detrimental to the ecosystem and eco-system. Physical and pharmacological methods are also frequently used. One recently changed moist chemistry method that has been used to create nanoscale nanoparticles is sol-gel autoignition. Reduced expense and energy consumption, improved control over crystallite size and stoichiometry, and uniform blending of reactants at the submicroscopic level are just a few of the special benefits that these methods provide [14].

Experimentation

Synthesis

High quality chemicals of zirconyl nitrate ($ZrO(NO_3)_2.xH_2O$), barium nitrate ($Ba(NO_3)_2$), ammonium nitrate (NH_4NO_3), and urea were used as starting reagents for the synthesis of $BaZrO_3$ perovskite nanoparticles. To create barium and zirconyl nitrate, deionized water was first used as a diluted solution. Following the addition of the barium nitrate solution and zirconyl nitrate solution, the first ammonium nitrate solution was added. The process of adding is continuously agitated. Previously, a mixture of Ba^{2+}, Zr^{4+}, and NH_4NO_3 was produced. In a similar manner, urea (acting as a fuel) was added. This entire solution quickly created an opal gel that, when heated for 10 h at 100 °C under an infrared lamp, totally dehydrated the substance. They were then burned in a muffle furnace for 10 min at 300 °C, resulting in a bulky, ash-colored material. Agate mortar and pestle were used to grind the ash-like product before it was progressively calcined at 600 °C for a few hours to produce crystalline white powder.

Results and Discussion

BZO:0.5Gd^{3+} samples' XRD patterns, to demonstrate their chemical phases, are shown in figure 1. All the diffraction peaks can be correlated to $BaZrO_3$'s cubic phase (JCPDS 06-0399). The doped sample showed no signs of any additional impurities, which suggests a homogeneous solid solution of $BaZrO_3$ and Gd^{3+}. Thus, it can be concluded that the host crystal structure of the BZO hosts did not significantly change or distort because of the doping of the Gd^{3+} ion. $BaZrO_3$ is a form of perovskite that has a perfect cubic structure, with barium atoms occupying the cube's corner position (000), zirconium atoms occupying the body's centre position (1/2, 1/2, 1/2), and oxygen atoms occupying the face's center positions (1/2,1/2,0). It is a part of the Oh point symmetry Pm3m space group. While barium is referred to as the lattice modifier and has a coordination number of 12 in the form of BaO_{12} cuboctahedra, zirconium is the lattice former and

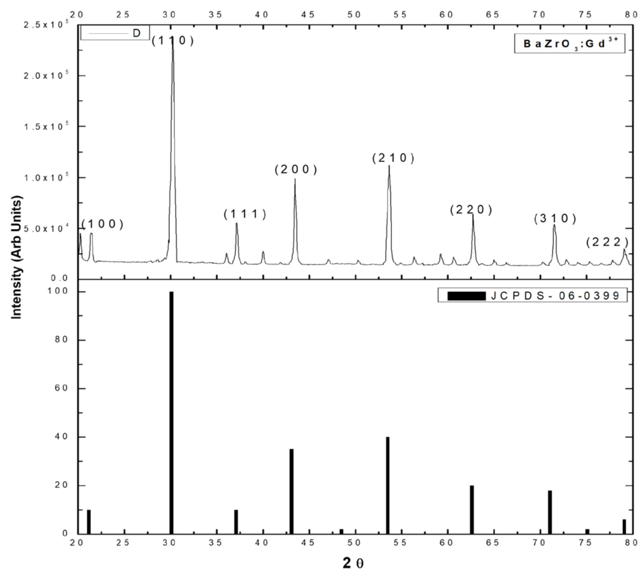

Figure 1: XRD pattern of $BaZrO_3$:Gd^{3+} doped phosphor.

has a coordination number of 6 oriented in the form of ZrO_6 octahedra. Corner connected ZrO_6 octahedra embedded inside a barium atom-formed cube represent the material's unit cell.

A study using SEM was done to look at the morphology of the synthetic phosphor powder. The SEM pictures of the $BaZrO_3:Gd^{3+}$ phosphors are shown in figure 2. The powder particles are strongly agglomerated, have a rough surface, pores, voids, and cracks, according to the SEM image. Additionally, it is obvious that the particles' sizes and shapes are asymmetrical and non-uniform. The non-uniform distribution of temperature and mass flow in the combustion flame is to blame for the irregular and non-uniform behavior of the particles. The image vividly demonstrates how pores, holes, and cracks emerge as a gas escape under high pressure together with the production of microscopic particles. Image demonstrates the interconnectedness of the particles, which is a feature of the combustion product. To confirm the produced phosphor's chemical composition, an energy dispersive X-ray (EDX) spectroscopy study was performed. Figure 2 displays the $BaZrO_3:Gd^{3+}$ EDX bands. It verifies that the phosphor contains all the necessary constituents of the target substance. Table 1 contains the chemical percentages of the elements that make up phosphor.

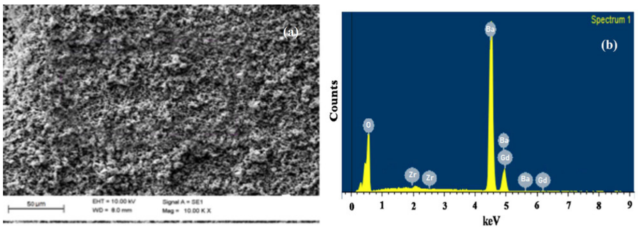

Figure 2: (a) SEM image and **(b)** EDX spectra of $BaZrO_3:Gd^{3+}$ doped phosphor

Table 1: Elemental composition of $BaZrO_3:Gd^{3+}$ doped phosphor.

S. No.	Elements	Weight %	Atomic %
1	Ba	65.63	33
2	Zr	22.02	16.66
3	O	11.58	0.5
4	Gd	0.759	0.33
Totals		99.99	99.98

Transmission electron microscope image of $BaZrO_3$ particles is shown in Figure 3. Smaller particles are scattered among agglomerated particles in the $BaZrO_3$ matrix, as seen in the image. Typically, the nanoparticles measure 20 to 30 nm. Additionally, we saw some huge particles that were between 60 and 100 nm in size.

Optical behavior

The $BaZrO_3:Gd^{3+}$ phosphor's excitation and emission spectra are depicted in figure 4a and figure 4b, respectively. When the emission wavelength is set at 318 nm, the excitation spectra display a band at 254 nm in the UV zone. The band results from the Gd^{3+} ions' 8S7/2 → 6DJ transition. The observed bands are connected to the Gd^{3+} ions' f-f transitions.

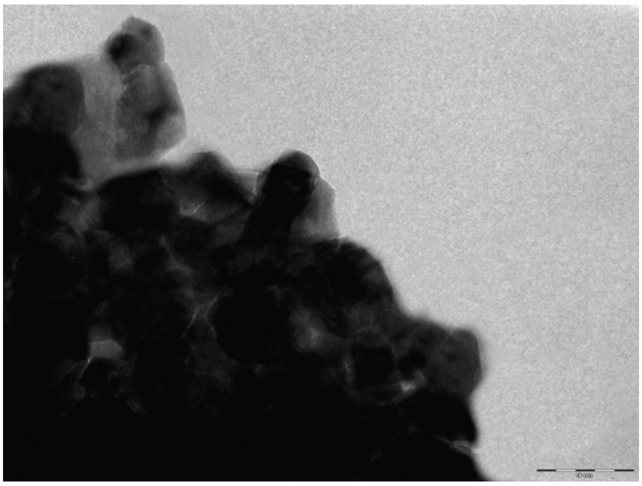

Figure 3: Transmission electron microscope image of $BaZrO_3:Gd^{3+}$ doped phosphor.

The band positions that were observed and their assignments correlate well with other band placements that have been reported [4,14]. Similar kind of excitation spectra for Gd doped $MgAl_2O_4$ phosphors was reported by Singh et al. [18]. When the emission is fixed at 312 nm, they noticed five bands in the excitation spectrum at 246, 253, 273, 276 and 279 nm. The 4f7 electrical arrangement is ground energy level to the ion Gd^{3+}. About 32000 cm^{-1} of energy separates the ground state from the first excited state. According to theoretical estimates, the Gd^{3+} ions' 4f7 energy levels can reach a maximum of 150000 cm^{-1}. Experimental reports on energy levels up to 67000 cm^{-1} have been made [19].

Due to significant UV absorption in the phosphor lattice, which masks all the absorption bands except for a few low-lying excited states, studies of Gd^{3+} ions in phosphors are limited. The $BaZrO_3:Gd^{3+}$ phosphor's emission spectrum is depicted in figure 4b when the excitation wavelength is set at 254 nm. A strong band at 318 nm, a somewhat strong band at 348 nm, and a weak band at 355 nm are all visible in this spectrum. These bands are the result of the transition of Gd^{3+} from its excited state (6PJ) to its ground state (8S7/2). This emission falls under the category of UVB, and it can be used in phototherapy lamps to treat a variety of skin conditions. The band placements that were observed and those reported in the literature agree well [17]. A 313 nm emission band in $Gd_2Zr_2O_7$ phosphor was discovered by Singh et al. [20] and identified as the 6P7/2 → 8S7/2 transition. Additionally, they [18] noticed an emission band in the emission spectrum of Gd doped $MgAl_2O_4$ phosphor at about 312 nm. The 6P7/2 → 8S7/2 transition has been implicated in the band at 318 nm,

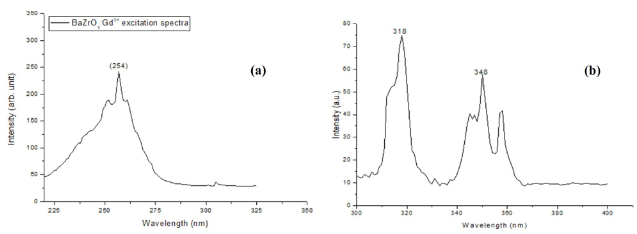

Figure 4: Photoluminescence excitation spectra of $BaZrO_3:Gd^{3+}$ monitored at **(a)** 615 nm and **(b)** 254 nm.

which is a phonon-assisted band. Research on phototherapy was done in the UV (270 - 320 nm) range by Parrish and Jaenicke [21]. They discovered that UV emission in a specific range between 300 and 320 nm had significant therapeutic effects while UV emission in the range between 270 and 300 nm was ineffective and even caused negative effects. The synthesized phosphor with a narrow band centred at 318 nm may be a possible candidate for use in phototherapy, according to the findings of the current investigation's photoluminescence tests. They discovered that UV emission in a specific range between 300 and 320 nm had substantial curative effects while UV emission in the range between 270 and 300 nm was ineffective and even caused adverse effects. According to this investigation's findings, the produced phosphor with a narrow band centred at about 318 nm might be a contender for use in phototherapy, as shown by the acquired photoluminescence results.

Effect of Gd^{3+} ion

The drug concentration of Gd^{3+} has a substantial impact on the photoluminescence efficacy of the samples. The light efficacy of Gd^{3+} increases quickly with rising amounts of gadolinium ions, up to 2 mol% content of Gd^{3+} doping ions, as is evident in figure 5. This is the occurrence known as concentration quenching, which occurs when the activator concentration goes above a certain threshold known as the critical concentration [18-23]. Over 2 mol% of gadolinium doping levels, the concentration quenching effect was seen in the current chapter. The proximity of the closest Gd^{3+} ions and contacts between them increase the likelihood of non-radiative energy transfer, which causes the concentration quenching effect, which reduces the light intensity (Figure 5). One of the following mechanisms, such as an exchange interaction or a multipole-multipole interaction, may be used to explain the energy transfer event that causes concentration quenching. Blasse proposed a measure termed critical distance to clarify and categorise the sort of contact mechanism (Rc). When Rc is determined to be higher than 5 Å, the multipole interaction takes precedence. Otherwise, the exchange contact will be the main method for energy transmission if the Rc number is less than 5 Å. The following formula can be used to determine the value of Rc:

Rc = [3V/4XcN]1/3

The effective number of Gd^{3+} sites per unit cell is denoted by N, the unit cell volume is denoted by V, and the critical activator concentration is denoted by Xc. N = 6, V = 74.75 Å^3, and Xc = 0.02 for the $BaZrO_3$:Gd^{3+} system. It is found that the current system's Rc number is 10.58 Å, which is considerably greater than 5 Å. The above finding indicates that the process of concentration reduction in the $BaZrO_3$:Gd^{3+} system is dominated by multipole-multipole interaction rather than exchange interaction [23].

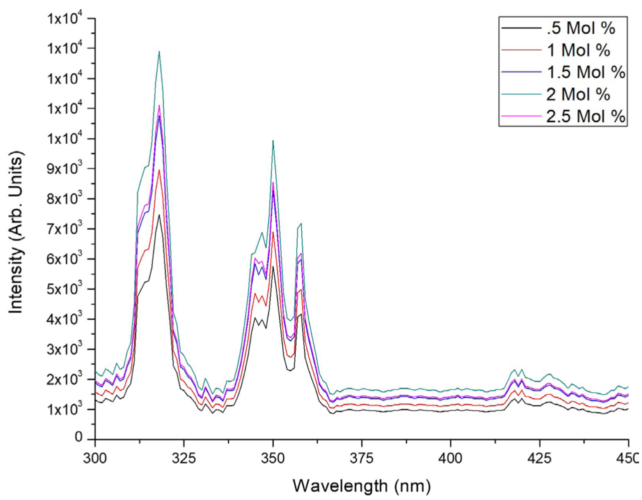

Figure 5: Photoluminescence spectra of $BaZrO_3$:Gd^{3+} (0.5 to 2.5 mol %).

Conclusion

The perovskite solar cell community commonly uses photoluminescence characterization, although the findings are difficult to understand and much remains to be learnt, such as the interaction between charge extraction and recombination. Photoluminescence-based measures lack standards, making it difficult to compare findings from various groups or compositions. This obscures how bulk, or interface kinetic characteristics relate to steady-state open-circuit voltage or other performance factors. By using urea combustion, it is possible to successfully manufacture gadolinium activated $BaZrO_3$ powder. The produced phosphor powder's XRD pattern shows that the crystal structure is entirely cubic. The transition 6PJ → 8S7/2 corresponds to the primary narrow UV emission band that has been seen at 314 nm (31847 cm^{-1}). $BaZrO_3$:Gd^{3+} phosphor is a strong contender for use in phototherapy lamps due to its UV emission. The maximum luminescence intensity was obtained for the $BaZrO_3$ samples with 2 mol% of Gd^{3+} contents. Above 2 mol% of Gd3t ions addition the concentration quenching phenomenon in tested phosphor takes place. The multipole-multipole interaction was estimated as the main mechanism responsible for luminescence quenching. The obtained photoluminescence results can be used for various solar cell application of the prepared phosphor.

Acknowledgments

None

Conflict of Interest

Authors declare that there is no conflict of interest.

References

1. Goulart CA, Boas LA, Morelli MR, de Souza DP. 2021. Reactive sintering of yttrium-doped barium zirconate ($BaZr_{0.8}Y_{0.2}O_{3-\delta}$) without sintering aids. *Ceram Int* 47(2): 2565-2571. https://doi.org/10.1016/j.ceramint.2020.09.102
2. Gong WP, Chen TF, Jin ZP. 2007. Thermodynamic investigation of ZrO_2-BaO system. *Trans Nonferrous Met Soc China* 17(2): 232-237. https://doi.org/10.1016/S1003-6326(07)60077-6
3. Singh V, Sivaramaiah G, Rao JL, Watanabe S, Rao TG, et al. 2015. New ultraviolet B emission from gadolinium activated $BaZrO_3$ phosphor - an electron paramagnetic resonance and optical study. *J Alloys Compd* 648: 1083-1089. https://doi.org/10.1016/j.jallcom.2015.07.025

4. Gupta SK, Pathak N, Kadam RM. 2016. An efficient gel-combustion synthesis of visible light emitting barium zirconate perovskite nanoceramics: probing the photoluminescence of Sm^{3+} and Eu^{3+} doped $BaZrO_3$. *J Lumin* 169: 106-114. https://doi.org/10.1016/j.jlumin.2015.08.032
5. Khirade PP, Raut AV, Alange RC, Barde WS, Chavan AR. 2021. Structural, electrical, and dielectric investigations of cerium doped barium zirconate ($BaZrO_3$) nano-ceramics produced via green synthesis: probable candidate for solid oxide fuel cells and microwave applications. *Phys B Condens Matter* 613: 412948. https://doi.org/10.1016/j.physb.2021.412948
6. Zhang Z, Xing FY, Zhu M, Zhu KL, Lu XG, et al. 2013. Vacuum induction melting of TiNi alloys using $BaZrO_3$ crucibles. *Mater Sci Forum* 765: 316-320. https://doi.org/10.4028/www.scientific.net/MSF.765.316
7. Chen G, Lan B, Xiong F, Gao P, Zhang H, et al. 2019. Pilot-scale experimental evaluation of induction melting of Ti-46Al-8Nb alloy in the fused $BaZrO_3$ crucible. *Vacuum* 159: 293-298. https://doi.org/10.1016/j.vacuum.2018.10.050
8. Bach M, Schemmel T, Hubálková J, Bühringer M, Jansen H, et al. 2021. Effect of thermal treatment conditions on the solid-state synthesis of barium zirconate from barium carbonate and monoclinic zirconia. *Ceram Int* 47(18): 25839-25845. https://doi.org/10.1016/j.ceramint.2021.05.313
9. Kuroha T, Yamauchi K, Mikami Y, Tsuji Y, Niina Y, et al. 2020. Effect of added Ni on defect structure and proton transport properties of indium-doped barium zirconate. *Int J Hydrogen Energy* 45(4): 3123-3131. https://doi.org/10.1016/j.ijhydene.2019.11.128
10. Imashuku S, Uda T, Nose Y, Taniguchi G, Ito Y, et al. 2008. Dependence of dopant cations on microstructure and proton conductivity of barium zirconate. *J Electrochem Soc* 156(1): B1.
11. Luo XY, Meng B, Zhao MY, Xie H, Bian LF, et al. 2019. Preparation and electrical conductivity of $BaZr_{0.8}Y_{0.2}O_{3-\delta}/(ZrO_2)_{0.92}(Y_2O_3)_{0.08}$ proton/oxygen ion conducting composite ceramic. *Ionics* 25: 1157-1165. https://doi.org/10.1007/s11581-018-2780-3
12. Khirade PP. 2019. Structural, microstructural, and magnetic properties of sol–gel-synthesized novel $BaZrO_3$-$CoFe_2O_4$ nanocomposite. *J Nanostruct Chem* 9: 163-173. https://doi.org/10.1007/s40097-019-0307-8
13. Ahmad T, Ubaidullah M, Lone IH, Kumar D, Al-Hartomy OA. 2017. Microemulsion synthesis, structural characterization and dielectric properties of $Ba_{1-x}Pb_xZrO_3$ ($0.05 \le x \le 0.20$) nanoparticles. *Mater Res Bull* 89: 185-192. https://doi.org/10.1016/j.materresbull.2017.01.044
14. Ahmad T, Ubaidullah M, Shahazad M, Kumar D, Al-Hartomy OA. 2017. Reverse micellar synthesis, structural characterization and dielectric properties of Sr-doped $BaZrO_3$ nanoparticles. *Mater Chem Phys* 185: 31-38. https://doi.org/10.1016/j.matchemphys.2016.10.001
15. Khirade PP, Birajdar SD, Humbe AV, Jadhav KM. 2016. Structural, electrical and dielectrical property investigations of Fe-doped $BaZrO_3$ nanoceramics. *J Electron Mater* 45: 3227-3235. https://doi.org/10.1007/s11664-016-4472-y
16. Liu Y, Zhang W, Wang B, Sun L, Li F, et al. 2018. Theoretical and experimental investigations on high temperature mechanical and thermal properties of $BaZrO_3$. *Ceram Int* 44(14): 16475-16482. https://doi.org/10.1016/j.ceramint.2018.06.064
17. Carnall WT, Fields PR, Rajnak K. 1968. Electronic energy levels of the trivalent lanthanide aquo ions. IV. Eu^{3+}. *J Chem Phys* 49(10): 4450-4455. https://doi.org/10.1063/1.1669896
18. Singh V, Sivaramaiah G, Rao JL, Kim SH. 2013. Luminescence and electron paramagnetic resonance investigation on ultraviolet emitting Gd doped $MgAl_2O_4$ phosphors. *J Lumin* 143: 162-168. https://doi.org/10.1016/j.jlumin.2013.03.054
19. Wegh RT, Donker H, Meijerink A, Lamminmäki RJ, Hölsä J. 1997. Vacuum-ultraviolet spectroscopy and quantum cutting for Gd^{3+} in $LiYF_4$. *Phys Rev* 56(21): 13841. https://doi.org/10.1103/PhysRevB.56.13841
20. Singh V, Sivaramaiah G, Rao JL, Kim SH. 2013. Optical and EPR studies of $Gd_2Zr_2O_7$ phosphors prepared via solution combustion method. *Phys B Condens Matter* 416: 101-105. https://doi.org/10.1016/j.physb.2013.02.012
21. Parrish JA, Jaenicke KF. 1981. Action spectrum for phototherapy of psoriasis. *J Invest Dermatol* 76(5): 359-362. https://doi.org/10.1111/1523-1747.ep12520022
22. Jeong H, Singh N, Pathak MS, Watanabe S, Rao TG, et al. 2018. Investigations of the ESR and PL characteristics of ultraviolet-emitting gadolinium-doped $ZnMgAl_{10}O_{17}$ phosphors. *Optik* 157: 1199-1206. https://doi.org/10.1016/j.ijleo.2017.11.108
23. Wyckoff RWG. 1931. Structure of Crystals. The Chemical Catalog Company, Inc. New York.